Synthesis, crystal structure determination, DFT calculation and Hirshfeld surface analysis of a new Zn(II) complex with the guaninium ligand

Kacim Klai, Christian Jelsch, Christine Lucas, Frédéric Lefebvre, Werner Kaminsky, Cherif Ben Nasr, Kamel Kaabi

Published in *Journal of Coordination Chemistry*, 2020, 1-15.
Doi : 10.1080/00958972.2020.1844192s

Synthesis, crystal structure determination, DFT calculation and Hirshfeld surface analysis of a new Zn(II) complex with the guaninium ligand

Kacim Klai[1], Christian Jelsch[2], Christine Lucas[3], Frédéric Lefebvre[3], Werner Kaminsky[4], Cherif Ben Nasr[1], Kamel Kaabi[1]*

[1] Laboratoire de Chimie des Matériaux, Université de Carthage, Faculté des Sciences de Bizerte, 7021 Zarzouna, Tunisie.

[2] CRM[2], CNRS, Institut Jean Barriol, Université de Lorraine, Vandœuvre les Nancy Cedex, France.

[3] Laboratoire de Chimie Organométallique de Surface (LCOMS), Ecole Supérieure de Chimie Physique Electronique, 69626 Villeurbanne Cedex, France.

[4] Department of Chemistry, BOX 351700 University of Washington Seattle, WA 98195, USA.

*Corresponding e-mail: kamel_kaabi@yahoo.fr

Graphical Abstract

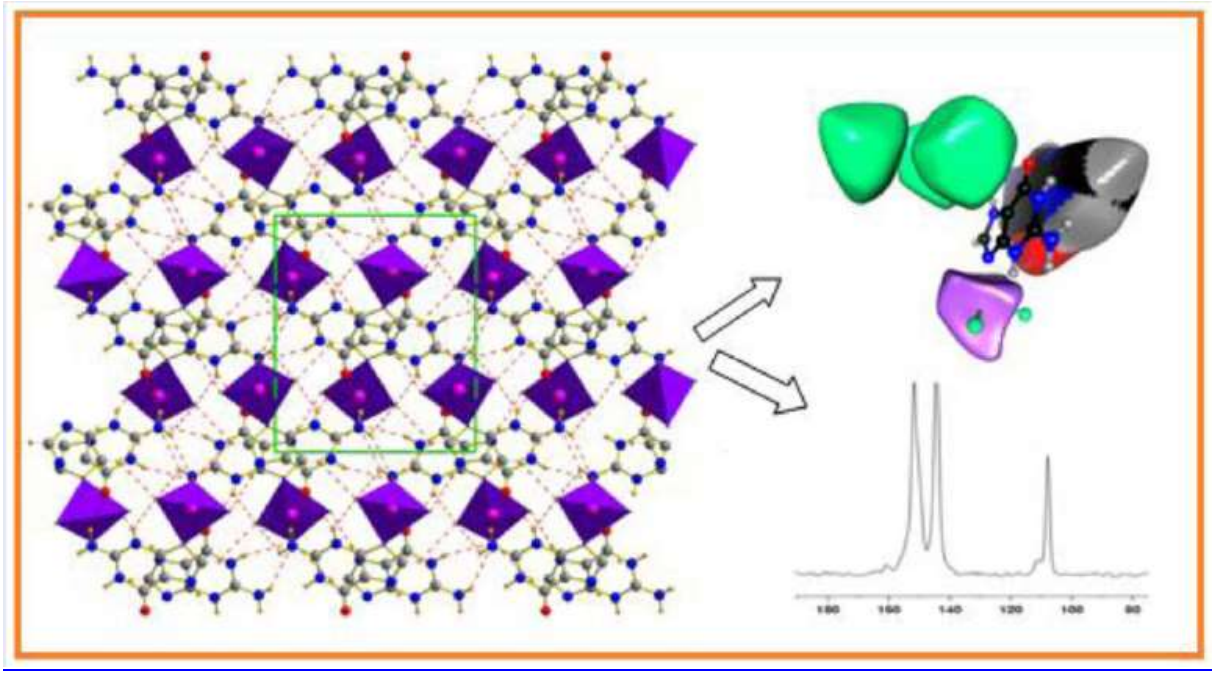

Abstract

A new Zn(II) complex with the guaninium monodentate ligand, $[ZnCl_3(C_5H_6N_5O)]$, has been synthesized in aqueous solution and studied by single crystal X-ray diffraction, elemental analysis, CP-MAS-NMR and IR spectroscopy. The Zn(II) atom is coordinated in a distorted tetrahedral fashion by three chloride anions and one nitrogen atom of the guaninium cation. The compound crystallizes in the monoclinic space group $P2_1/n$ with lattice parameters a = 8.8411(7), b = 11.7176(5), c = 10.3765(8) Å, β = 100.069(4) °, V = 1058.41(13) Å^3 and Z = 4. Intermolecular interactions were investigated by Hirshfeld surfaces. Besides the Zn(II) cation coordination, the crystal packing is stabilized by intermolecular N-H...O, N-H...Cl^- and C-H...Cl^- hydrogen bonds and C…C aromatic stacking which link the molecules into a three-dimensional network. The regions of strongest negative electrostatic on the Hirshfeld surface of guaninium ligand interact with electronegative atoms and vice versa. The ^{13}C and ^{15}N CP-MAS NMR spectra are discussed and the vibrational absorption bands were identified by infrared spectroscopy. The HOMO and LUMO energies and Molecular Electrostatic Potential surface were derived from DFT theoretical calculations.

Keywords: Coordination compound; X-ray diffraction; Hirshfeld surface; CP-MAS-NMR spectroscopy; DFT calculations.

1. Introduction

Over the past decades, there has been a sizable research effort on rational design and elaboration of transition-metal complexes due to their interesting structural, chemical, and physical properties such as storage of gas, separation of molecules, catalyzing the chemicals and delivery of drugs [1-5]. The interaction between divalent metal cations and nucleic acids has also been widely studied due to their importance for DNA replication, transcription and metabolic processes [6-11]. It is well known that metal atoms that interact with nucleobases in DNA and RNA can modify hydrogen bonds and cause DNA oxidation, thereby affecting the formation of the double helix and causing mutation points. [12,13]. Metal ions can bind directly to nucleic acid bases via the oxygen or nitrogen atoms of the bases. Guanine is one of the purine bases that take place into the composition of nucleic acids (DNA or RNA) and carry their genetic

information. In this context, the molecular architecture of transition-metal complexes containing nucleobases is very useful, giving various molecular geometric shapes and high-dimensional architectures [14]. The chemistry of zinc compounds is gaining a great attention due to their interesting structural features, catechol oxidase, schizonticidal, antimalarial, antimicrobial, tumor photosensitizers and their potential use as agricultural biocides [15–18]. When considering biologically relevant transition metals, zinc is the second most abundant element found within cells, behind iron. Zinc ions (Zn^{2+}) are known to facilitate diverse protein functions that are essential for life [19].

In this context, we describe here the synthesis, growth, structure, Hirshfeld surface analysis and spectroscopic (FT-IR, ^{13}C and ^{15}N NMR) characterization of a new Zn(II) salt complex with the guaninium ligand.

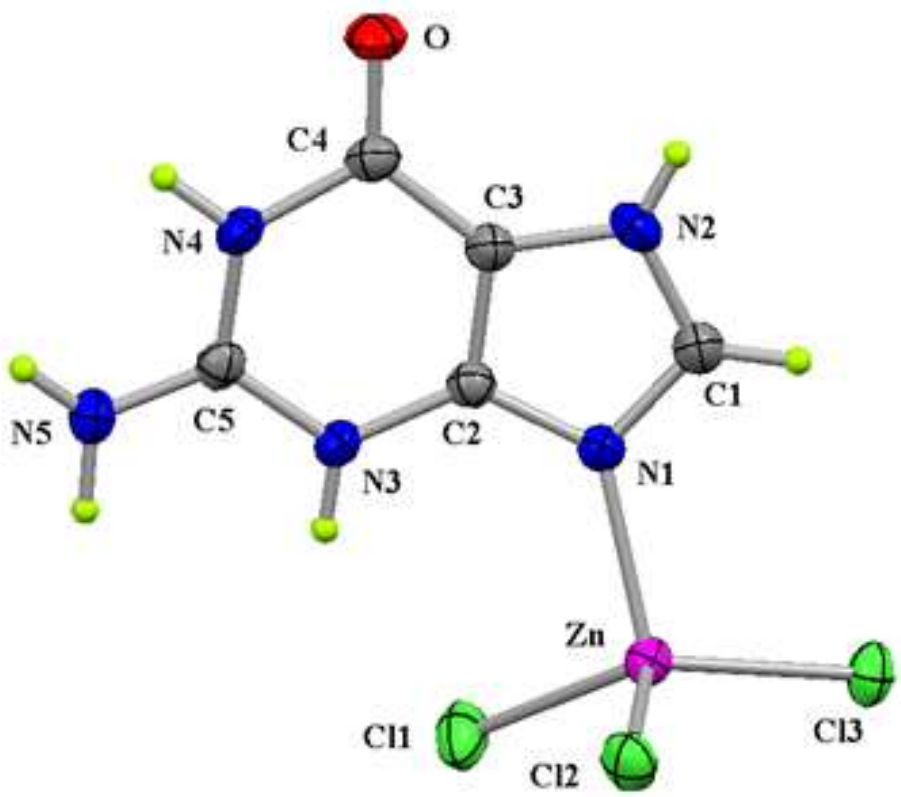

Figure 1 ORTEP of the title compound with thermal displacement ellipsoids drawn at the 40% probability level

2. Experimental

2.1. Chemical preparation

The synthesis of [$ZnCl_3(C_5H_6N_5O)$] was carried out by addition of a solution of guanine hydrochloride (0.2 mmol) in methanol–water medium [60.40 v/v] (10 mL) to a solution of $ZnCl_2$ (0.2 mmol) in 5 mL of methanol. The mixture was then stirred for 40 min at room temperature. The resulting solution was filtered and the filtrate was kept at room temperature for slow evaporation. After a few days, dark green crystals suitable for X-ray diffraction were obtained (yield 68 %). Anal. Calc.: C, 18.53 %; H, 1.85 %; N, 21.16 %. Found: C, 18.32 %; H, 1.92 %; N, 21.46 %.

2.2. Investigation techniques

2.2.1. X-ray single crystal structural analysis

A dark green prism measuring 0.25 x 0.15 x 0.12 mm^3 was mounted on a loop with oil. Data were collected at 294 K on a Nonius Kappa CCD FR590 single crystal X-ray diffractometer using the Mo-radiation. The crystal-to-detector distance was 30 mm and the exposure time was 90 seconds per degree for all sets. The scan width was 2°. Data collection was 99.9% complete to 25° in θ. A total of 4573 merged partial and complete reflections were collected covering the indices, -11<=*h*<=11, -13<=*k*<=15, -13<=*l*<=13. 2610 reflections were symmetry independent and the value of R_{int} = 0.0351 indicated that the data set was excellent. Indexing and unit cell refinement indicated a primitive monoclinic lattice. The space group was found to be $P2_1/n$ (N°. 14). The data were integrated and scaled using hkl-SCALEPACK [20]. This program applies a multiplicative correction factor (*S*) to the observed intensities (I) and has the following form:

$$S = (e^{-2B(\sin^2\theta)/\lambda^2}) / \text{scale}$$

S is calculated from the scale and the *B* factor is determined for each frame and is then applied to *I* to give the corrected intensity (I_{corr}).

Solution by direct methods (SHELXS, SIR97 [21]) produced a complete heavy atom phasing model consistent with the proposed structure. The structure was completed by difference Fourier synthesis with SHELXL [22, 23]. Scattering factors were from Waasmair and Kirfel [24]. Hydrogen atoms were placed in geometrically idealized positions and constrained to ride on their parent atoms with C---H distances in the range 0.95-1.00 Å. Isotropic thermal parameters U_{iso} were fixed in such a way that they were 1.2.U_{eq} of their parent atom for CH groups and 1.5.U_{eq} of their parent atom for methyl groups. All non-hydrogen atoms were refined anisotropically by full-matrix least-squares.

Supplementary data

Crystallographic data for the structural analysis have been deposited at the Cambridge Crystallographic Data Centre, CCDC No 1993138. These data can be obtained free of charge via http://www.ccdc.cam.ac.uk/conts/retrieving.html, or from the CCDC, 12 Union Road, Cambridge, CB2 1EZ, UK: fax: (+44) 01223-336-033; e-mail: deposit@ccdc.cam.ac.

2.2.2. NMR and IR measurements

The NMR spectra were recorded on a solid-state high-resolution Avance-300 spectrometer operating at 75.49 MHz for ^{13}C and 30.30 MHz for ^{15}N with a classical 4 mm probe head allowing spinning rates up to 10 kHz. ^{13}C and ^{15}N NMR chemical shifts are given relative to tetramethylsilane and liquid ammoniac, respectively (precision 0.5 ppm). The spectra were recorded by use of cross-polarization (CP) from protons (contact time 2 ms) and magic angle spinning (MAS). Before recording the spectra, it was checked that there was a sufficient

delay between the scans allowing a full relaxation of protons. The IR spectrum was recorded in the 4000-400 cm^{-1} range using a NICOLET IR 200 FT-IR infrared spectrometer.

Table 1. Crystal data and structure refinement of $[ZnCl_3(C_5H_6N_5O)]$.

Crystal data	
Chemical formula	$C_5H_6Cl_3N_5OZn$
M_r	323.87
Crystal system, space group	Monoclinic, $P2_1/n$
Temperature (K)	294
a, b, c (Å)	8.8411 (7), 11.7176 (5), 10.3765 (8)
β (°)	100.069 (4)
V (Å^3)	1058.41 (13)
Z	4
Radiation type	Mo $K\alpha$
μ (mm^{-1})	3.06
Crystal size (mm)	0.25 × 0.15 x 0.12
Data collection	
Diffractometer	Kappa CCD
No. of measured, independent and	4573, 2610, 2028
R_{int}	0.035
$(\sin\theta/\lambda)_{max}$ (Å^{-1})	0.667
Refinement	
$R[F^2 > 2\sigma(F^2)]$, $wR(F^2)$, S	0.033, 0.078, 1.06
No. of reflections	2610
No. of parameters	151
$\Delta\rho_{max}$, $\Delta\rho_{min}$ (e Å^{-3})	0.64, −0.48
CCDC number	1993138

Table 2. Selected bond distances and angles (Å, º) in $[ZnCl_3(C_5H_6N_5O)]$.

N1—Zn1	2.052 (2)	N1—Zn1—Cl1	102.93 (6)
Cl1—Zn1	2.2304 (8)	N1—Zn1—Cl3	108.23 (6)
Cl2—Zn1	2.2614 (7)	Cl1—Zn1—Cl3	118.57 (3)
Cl3—Zn1	2.2408 (7)	N1—Zn1—Cl2	103.01 (6)
C1—N1	1.339 (3)	Cl1—Zn1—Cl2	108.22 (3)
C1—N2	1.330 (3)	Cl3—Zn1—Cl2	114.14 (3)
C2—N1	1.359 (3)	N2—C1—N1	111.8 (2)
C2—C3	1.368 (3)	N1—C2—C3	110.6 (2)
C2—N3	1.369 (3)	N1—C2—N3	127.1 (2)
C3—N2	1.369 (3)	C3—C2—N3	122.3 (2)
C3—C4	1.409 (4)	C2—C3—N2	105.4 (2)
C4—O1	1.213 (3)	C2—C3—C4	122.6 (2)
C4—N4	1.417 (3)	N2—C3—C4	132.0 (2)
C5—N5	1.294 (3)	O1—C4—C3	128.3 (3)
C5—N4	1.349 (3)	C3—C4—N4	110.7 (2)
C5—N3	1.351 (3)	N5—C5—N4	120.7 (2)
C1—N1—C2	104.6 (2)	N5—C5—N3	120.5 (2)
C1—N2—C3	107.6 (2)	N4—C5—N3	118.7 (2)
C5—N3—C2	118.4 (2)	C5—N4—C4	127.3 (2)

3. **Results and discussion**

3.1. X-ray diffraction study

The main geometrical features of the different chemical entities of $[ZnCl_3(C_5H_6N_5O)]$ are given in Tables 2 and 3. X-ray crystal structure analysis reveals that this coordination compound crystallizes in the monoclinic space group $P2_1/n$. The asymmetric unit of the compound comprises one Zn(II) cation, three chloride anions Cl^- and one monodentate guaninium ligand (Fig. 1). The Zn(II) atom is coordinated in a distorted tetrahedral fashion by three chloride anions Cl^- and one nitrogen atom of the guaninium ligand. The detailed geometry of the $ZnCl_3N$ tetrahedron (Table 2) shows that the bond distances, Zn–Cl1 = 2.2304(8) Å, Zn–Cl2 = 2.2614(7) Å, Zn–Cl3 = 2.2408(7) Å and Zn–N1 = 2.052(2) Å are comparable to those observed in other similar Zn(II) complexes [25-27]. The bond angles around the Zn atom range

from 102.93 (6) to 118.57 (3) indicating that the $ZnCl_3N$ species has a slightly distorted tetrahedral geometry. The average values of the distortion parameters of the $ZnCl_3N$ tetrahedron were quantified using equations (1) and (2) [28].

$$ID(\text{Zn–X}) = \sum_{i=1}^{n1} \frac{|di-dm|}{n1.dm} \qquad (1)$$

$$ID(\text{X-Zn-X}) = \sum_{i=1}^{n2} \frac{|\alpha i-\alpha \ |}{n1.\alpha m} \qquad (2)$$

(X = Cl1, Cl2, Cl3 or N1)

Where *d* is the Zn-X bond distance, α the X–Zn–X bond angle, *m* the average value, n_1 =4 and n_2 = 6. The values of the distortion indices were *ID*(Zn–X) = 0.033 and *ID* (X–Zn–X) = 0.043. These low values of the distortion indices indicate that the coordination geometry of the Zn atom is a slightly distorted tetrahedron.

The projection along the direction of the **a**-axis of the structure of $[ZnCl_3(C_5H_6N_5O)]$ shows that it contains a network of three-dimensional hydrogen bonds due to the large abundance of donors and acceptors of hydrogen bonds (Fig. 2). This projection also shows that the $ZnCl_3N$ polyhedra are arranged in chains parallel to **c**-axis which cross the unit cell at *y* = ¼ and *y* = ¾, the organic residues being located between them. Each molecule of the complex is linked to the four neighboring nearest molecules that surround him by hydrogen bonds of C-H... Cl, N-H...Cl and N-H...O type to form corrugated layers parallel to the (**b**, **c**) plane (Figs. 2 and S1, Table 3). These layers are located at z = *n*+ ½ and interconnect through C1–H1...Cl1 and N5–H5A…Cl1 hydrogen bonds. The amine -NH_2 and the -C1H groups participate as H-bonding donors and the Cl1 chlorine atoms participate as H-bonding acceptor to form a three-dimensional network (Fig. 3). Figure 3 shows the overall packaging pattern in which the different components of the material studied are arranged so as to create two types of channels, the largest one of lozenge form of center (0, 0, 0) and (½, ½, 0) and the other smallest square

shaped and centered at (0, ½,0) and (½, 0, 0). All these channels extend along the **c**-axis and are arranged alternately in the direction of the ***a*** and ***b*** axes. The planar guaninium cycles form stacking chains along the **a**-axis, two interacting cycles being related via an inversion centre (Fig. 3 and S2).

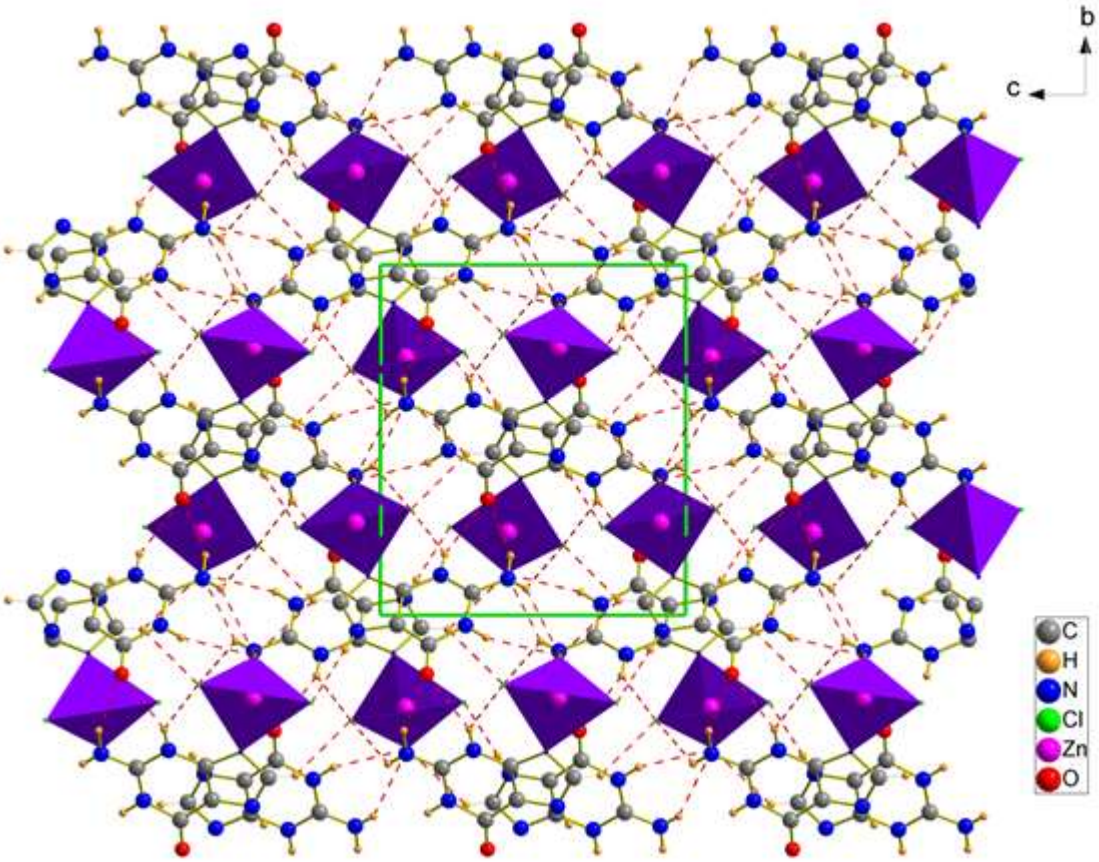

Fig. 2 A projection of the structure of [$ZnCl_3(C_5H_6N_5O)$] along the *a*-axis. Dotted lines indicate hydrogen bonds.

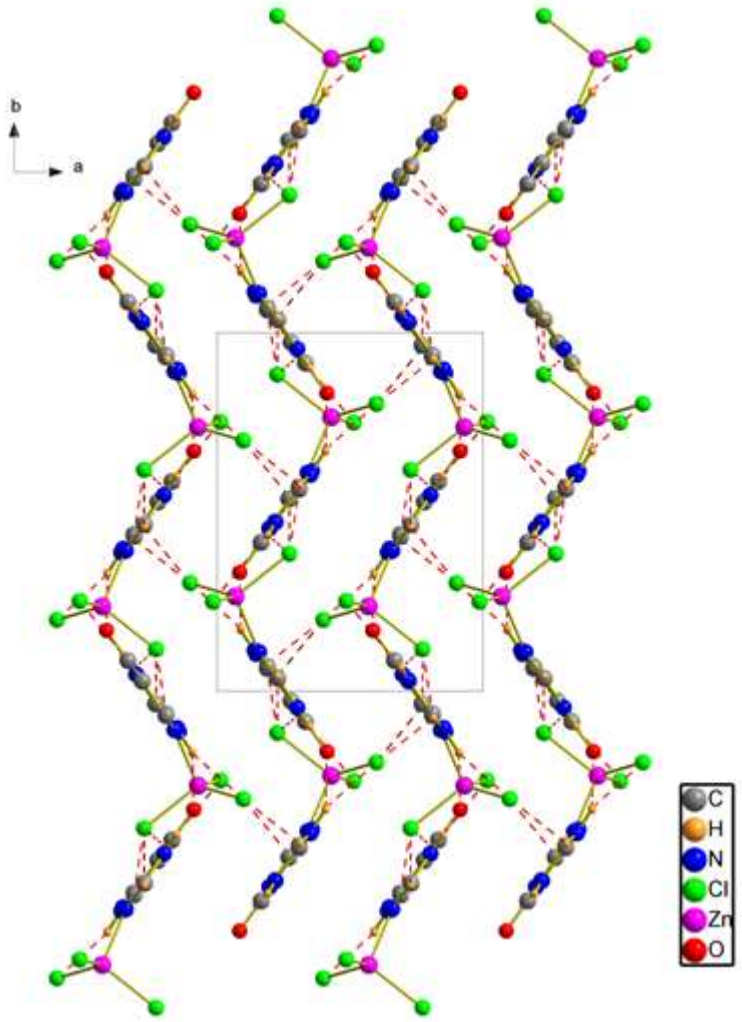

Fig. 3 Projection of the structure of [$ZnCl_3(C_5H_6N_5O)$] along the *c*-axis. Dotted lines indicate hydrogen bonds.

It is worth noting that, due to the tautomerism phenomenon, the guanine can be found in its two following forms:

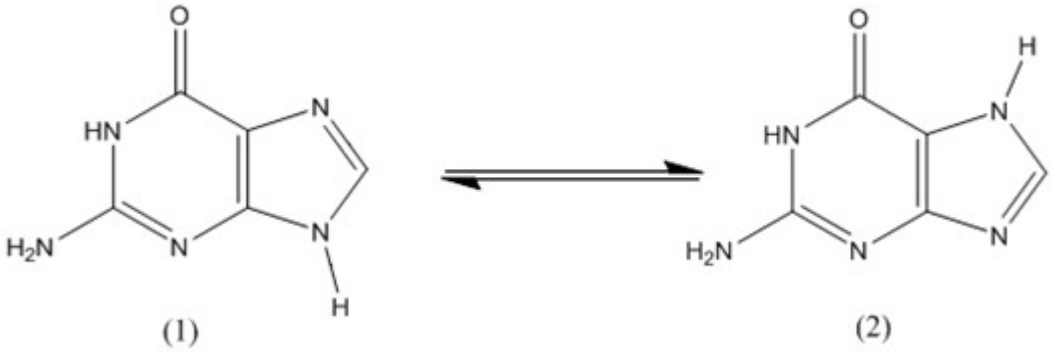

In the present case, the starting reagent is present as the form (2) since the nitrogen atom bonded to the Zn^{2+} ion is not protonated (Fig. 1). The protonation and coordination of the base are similar to that found in a trichloroguaniniumizinc (II) and trichloroguaniniumicopper (II) [25, 29]. The distances and angles of the bonds describing the organic cation are grouped together in Table 2. They all correspond to values usually found in the literature [25, 29-31].

Table 3. Hydrogen-bond geometry (Å, º) of $[ZnCl_3(C_5H_6N_5O)]$.

Symmetry code : (i) x+ ½ , −y+½, z+½; (ii) −x+½, y−½, −z+½; (iii) −x+½, y+½, −z−½; (iv) −x+½, y−½, −z−½; (v) x+½, −y+½, z−½.

D—H···*A*	*D*—H	H···*A*	*D*···*A*	*D*—H···*A*
C1—H1···Cl1^{i}	0.93	2.87	3.510	127
C1—H1···Cl2^{ii}	0.93	2.72	3.422	133
N2—H2···Cl3^{ii}	0.811	2.453	3.260	173.63
N3—H3···Cl1	0.839	2.659	3.347	140.17
N3—H3···O1^{iii}	0.839	2.343	3.000	135.55
N4—H4···Cl2^{iv}	0.873	2.574	3.327	145.09
N5—H5A···Cl1^{v}	0.832	2.841	3.356	121.85
N5—H5A···Cl2^{iv}	0.832	2.582	3.277	141.87
N5—H5B···O1^{iii}	0.922	2.052	2.833	121.65

Table 4. Analysis of contacts on the Hirshfeld surface. Reciprocal contacts X…Y and Y…X are merged. The second line shows the chemical content on the surface. The % of contact types between chemical species is given followed by their enrichment ratio. The major contacts as well as the major enriched ones are highlighted in bold characters. The hydrophobic hydrogen atoms bound to carbon (Hc) were distinguished from the more polar one bound to nitrogen (Hn). Hydrophobic contacts are in italics.

atom	Cl	Zn	Hn	O	N	Hc	C
%	39.6	12.6	16.7	5.2	8.8	*3.7*	*13.5*
Cl	4.4						
Zn	**22.5**	0.0					
Hn	**23.6**	1.6	0.3				
O	2.7	0.0	5.0	0.0			
N	6.1	5.5	0.2	0.1	0.4		
Hc	6.3	0.1	0.1	0.0	0.1	*0.0*	
C	**10.0**	2.9	1.1	2.1	2.5	*0.1*	*2.2*
Cl	0.27						
Zn	**1.72**	0					
Hn	**1.84**	0.31	0.10				
O	0.67	0	**3.2**	0			
N	1.00	**2.13**	0.07	0.19	0.67		
Hc	**2.34**	0.12	0.08	0	0.2	*0*	
C	1.08	0.74	0.29	**1.84**	**1.44**	*0.14*	***1.71***

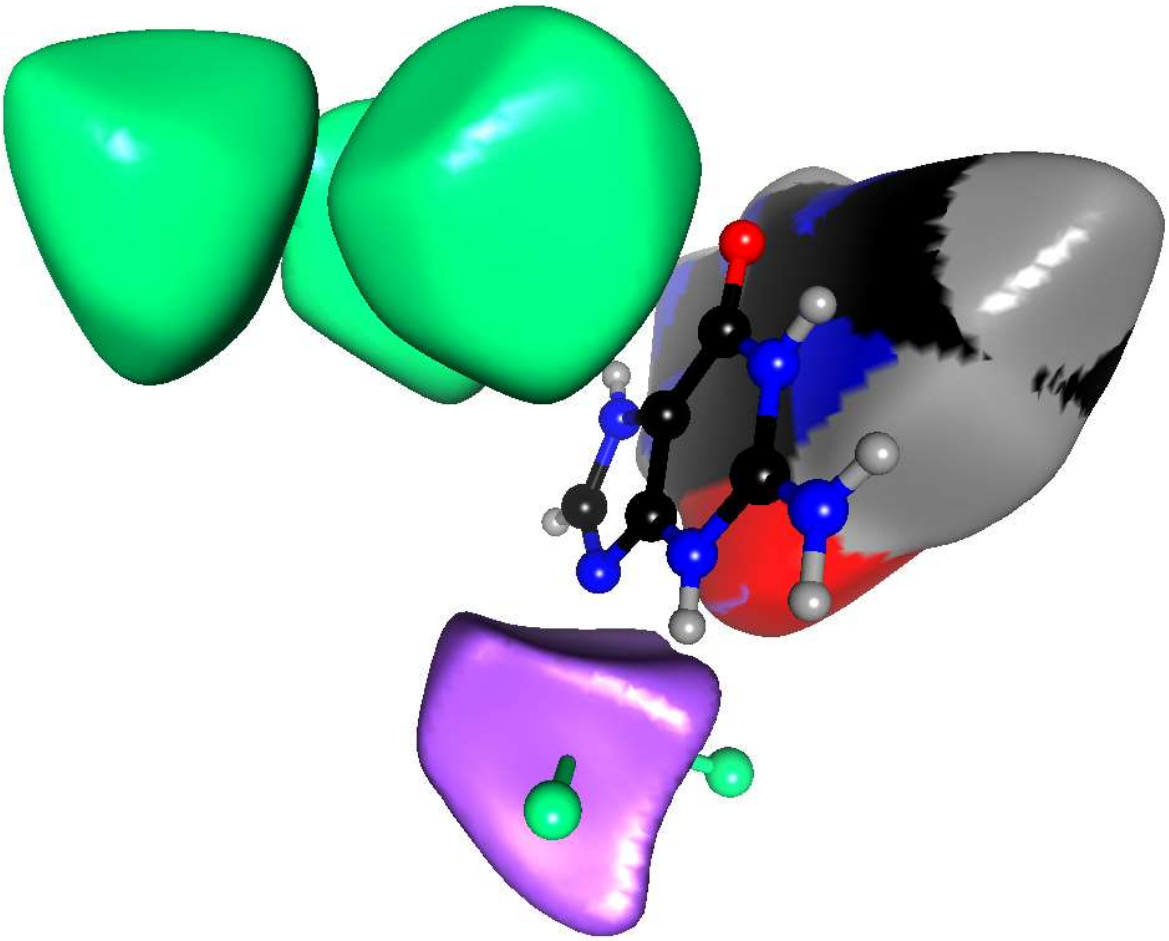

Figure 4. View of Hirshfeld surface around the moieties constituting the asymmetric unit. The surface is colored according to the atom type: black: carbon, red: oxygen, blue: nitrogen, purple: zinc,gray: Hc, light blue: Hn.

3.2. Hirshfeld contacts

The different contact types and their enrichment (Table 4) in the crystal packing were also analyzed with MoProViewer software [32]. The enrichment ratio E_{XY} for a pair of elements (X,Y) is defined as the ratio between the proportion of actual contacts *C*xy in the crystal and the theoretical proportion *R*xy of equi-distributed random contacts [33]. In order to obtain integral Hirshfeld surfaces around all entities, molecules not in contact with each other in the crystal were selected (Fig. 4). An enrichment ratio larger than unity reveals that a contact type is over-represented in the crystal; while pairs that tend to avoid contacts with each other should yield an *E* value lower than unity.

The fingerprint plots of the contacts at Hirshfeld surface around asymmetric shown in Fig. S3) were generated with software CrystalExplorer3.1 [34]. The inner spikes at short contact distance represent the O…H hydrogen bonds while the outer spikes are due to the H…Cl^- H-bonds.

The Zn^{++}…Cl^- coordination and the Hc…Cl^- weak hydrogen bonds represent the most abundant contacts in the crystal (Table 4). Globally the hydrogen bonds (H…Cl, H…O and H…N) represent 35% of the contact surface.

The Hn…O strong hydrogen bond is the most enriched contact (*E*= 3.2). The Hc…Cl^- contact represents the second most favored, this is due to two incidental weak C-H…Cl^- hydrogen bonds. The Zn…Cl^- and Zn…N coordination contacts and over-represented as well as the strong Hn…O H-bonds. It is noteworthy that the stacking interaction of the flat guaninium results in enriched C…C, C…N and C…O contacts.

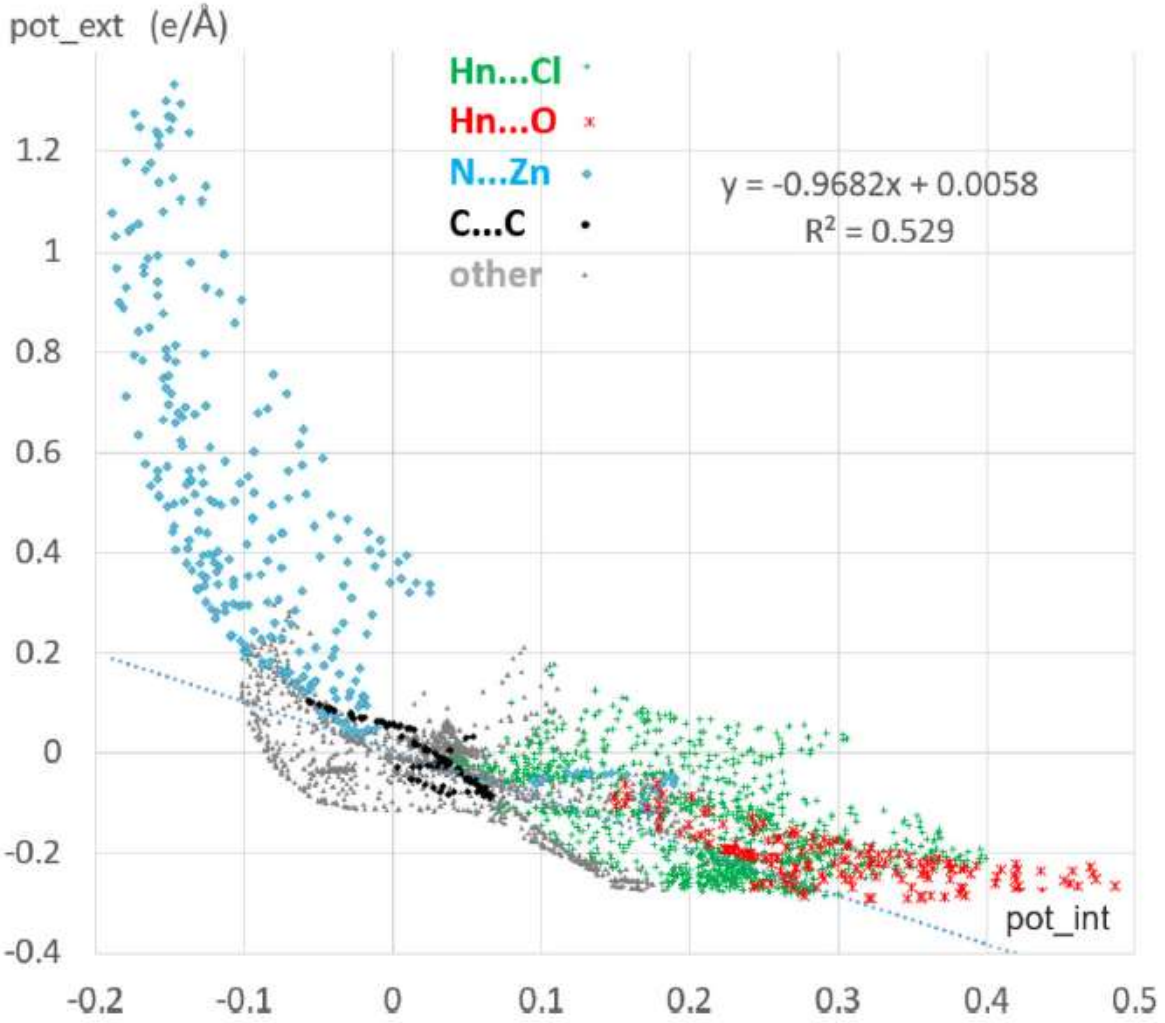

Figure 5. Scatter plot of the inner and external electrostatic potential around the guanidinium ligand, derived from multipolar atom model. The ext potential is generated by the first neighboring molecules in contact with the ligand. The main contacts are highlighted in color.

The electrostatic potential (ESP) was computed on the Hirshfeld surface of the guaninium using MoProSuite software [35]. The charge density of the title compound was modelled using the multipolar atom of Hansen & Coppens. The electron density parameters were transferred from the experimental ELMAM2 database of multipolar atoms [36]. After transfer on all other atoms, the number of valence electrons of the Zn cation was set 1.4 e to ensure electroneutrality. Fig. 5 highlights the good complementarity of the ESP generated by the guaninium and its immediate surrounding. The internal and external ESPs are anticorrelated with r = -0.73. The regions with most positive interior ESP values correspond to the Hn atoms forming Hn…O and

Hn…Cl hydrogen bonds with the most negative external ESP. On the other side of the scatterplot, the surface near N atom has the most electronegative ESP and is involved in the N…Zn(II) coordination with most positive external ESP.

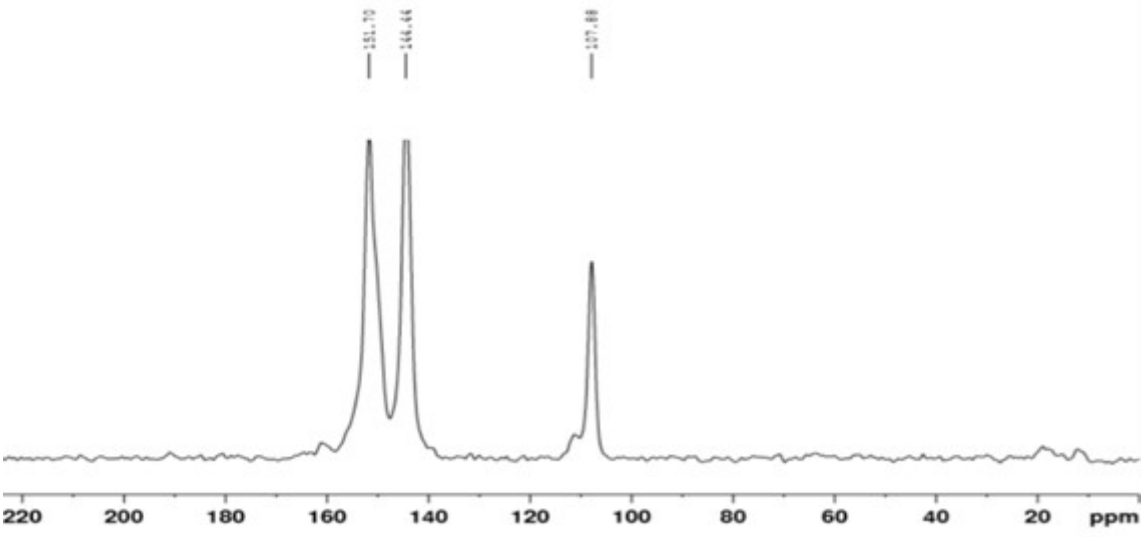

Figure 6. ^{13}C CP-MAS NMR spectrum of $[ZnCl_2(C_6H_9N_3O_2)]$.

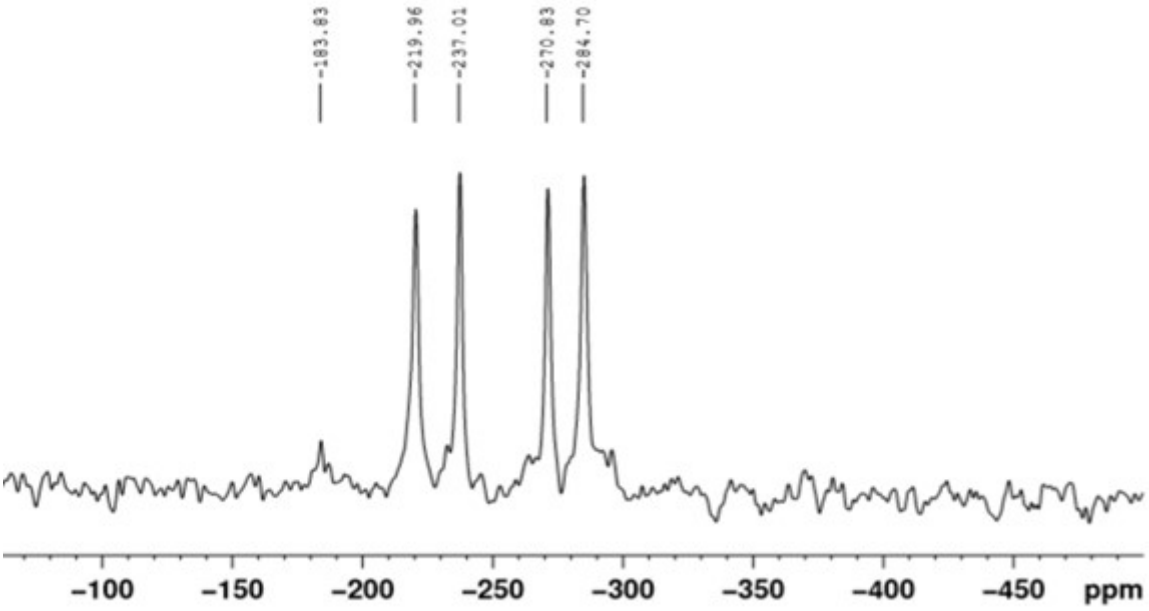

Figure 7. ^{15}N CP -MAS NMR spectrum of $[ZnCl_2(C_6H_9N_3O_2)]$.

3.3. NMR results

The ^{13}C CP-MAS NMR spectrum obtained for the title compound is displayed on Fig. 6. It shows three well-resolved resonance peaks corresponding to the five aromatic carbon atoms of the organic entity. In the resonance region of the C2-C5 aromatic carbons of the 6-membered ring in the guaninium (between 140 and 160 ppm), only two peaks are resolved corresponding to the four aromatic carbon atoms. This is probably due to the fact that the signals overlap in pairs. The peak at 108 ppm is attributed to the C1 carbon atom.

The ^{15}N CP-MAS NMR spectrum of $[ZnCl_3(C_5H_6N_5O)]$, presented in Fig. 7, is in good agreement with the structure determined by X-ray diffraction. It exhibits five well-resolved peaks corresponding to the five crystallographic independent nitrogen sites, which proves the presence of a single organic moiety in the asymmetric unit of the compound. The small peak appearing at -184 ppm corresponds to the N1 nitrogen atom. Its intensity is lower as there is no proton around it. The three peaks at -220 and -237 and -271 ppm correspond to the N2, N3 and N4 atoms. The peak at -285 ppm corresponds to the N5 aliphatic nitrogen atom.

Theoretical calculations were undertaken in order to assign the NMR resonances to the different crystallographic non-equivalent carbon and nitrogen atoms of the unit cell and confirm the above assignments. These calculations were made at the B3LYP/6-311+G* level after optimization of the positions of protons, the other atoms being at the X-ray positions. The different atoms are labeled as in Fig. 1.

The results are listed on Table 5. Clearly, there is a very good agreement between the experimental and the theoretical values calculated after optimization of the position of the protons, allowing unambiguously the attribution of the different NMR signals, even though

some calculated values for the isotropic chemical shifts are far away from the experimental ones.

Table 5. Comparison of calculated and experimental chemical shifts of carbon and nitrogen atoms in $[ZnCl_3(C_5H_6N_5O)]$.

Atoms	δ Calculated (ppm)	δ Experimental (ppm)
C1	150.5	144.4
C2	151.0	151.7
C3	110.3	107.9
C4	151.2	151.7
C5	148.9	144.4
N1	-127	-183.8
N2	-224	-220.0
N3	-248	-270.8
N4	-226	-237.0
N5	-304	-284.7

3.4. Quantum mechanical study

Quantum chemical calculation was performed from the crystal structure with DFT method at the 6-311+G* basis set, by using the Gaussian 09 program [37]. The HOMO and LUMO of the complex are shown in Fig. 8. It is clear that the HOMO is located mainly on the chlorine atom, while the LUMO is located on the organic ligand. The energies of HOMO and LUMO are −5.93 eV and −3.23 eV, respectively. The energy gap is 2.72 eV, a value which is relatively small indicating that the title material has a semiconductor behavior. The energy distribution of the different orbitals is shown in Fig. S4.

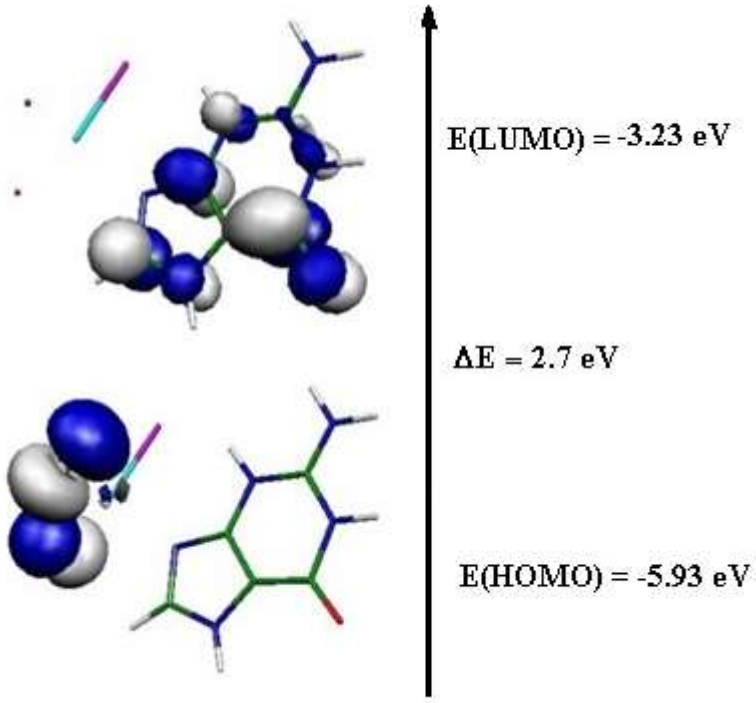

Figure 8 Frontier orbitals in $[ZnCl_2(C_6H_9N_3O_2)]$.

3.5. Molecular Electrostatic Potential analysis (MEP)

The Molecular Electrostatic Potential (MEP) surface is depicted in Fig. S5. The MEP is used to determine the nuclear and electronic charge distribution of a given molecule. The maps

were obtained at the B3LYP/6-311+G* level of theory. As it can be seen, the electrostatic potential maps are color-coded and are subdivided into many regions where those various colors are used to identify different potentials. Blue and red colors indicate the positive and negative potentials, respectively. The most negative zones are on the oxygen and chlorine atoms, while the most positive ones are located at the NH groups.

3. 6. IR spectroscopy

IR Spectroscopy was used to verify the functional groups present in the compound and to investigate their vibrational behavior in the solid state. The attributions of the observed bands are based on comparisons with data reported previously for similar materials [38–42] and on DFT calculations. The very large bands in the 3500-3200 and 3190-2900 cm^{-1} high-frequency regions (Fig. S6-a) are assigned to the stretching vibrations of the N H and C-H groups interconnected by a system of hydrogen bonds in the crystal, respectively [39]. The intense band at 1733 cm^{-1} can be attributed to the C=O groups of the organic ligand [41, 42]. The bands between 1680 and 1550 cm^{-1} correspond to the stretching vibrations of C=C and C=N groups and to the N-H bending vibration modes [43, 44]. The bands of medium intensities observed between 1400 and 1300 cm^{-1} are associated to the C–H *asymmetric and symmetric* bending *vibrations*. The observed bands in the 1200-1000 cm^{-1} range can be attributed to the bending vibrations of the C=C, C=N and C-C groups. Bands in the 1000 -500 cm^{-1} region correspond to the CH_3 rocking modes [45] and to the out of plane bending modes of the skeleton of the organic ring [46, 47].

The infrared spectrum of $[ZnCl_3(C_5H_6N_5O)]$ was also calculated by use of the B3LYP/6-311+G* method on the geometry obtained after optimization of the protons. The resulting IR spectrum between 4000 and 400 cm^{-1} is shown on Fig. S6-b and is very similar to the experimental one. A close agreement between the experimental and theoretical wave umbers

(R^2 = 0.9957) is mostly achieved in the finger-print region (Fig. S7). Thus, the precision is well-sufficient to assign the experimental frequencies and to confirm the attributions proposed above.

4. Conclusion

The synthesis and characterization of the new coordination compound, [$ZnCl_3(C_5H_6N_5O)$], has been described. In this monomeric complex, Zn(II) atom is surrounded in a distorted tetrahedral fashion by three chloride anions and one nitrogen atom of the guaninium ligand. The intermolecular cohesion is essentially ensured by intermolecular N-H...O, N-H...Cl and C-H...Cl hydrogen bonds and C…C aromatic stacking. These attractive interactions are all over-represented in the crystal packing. The numbers of ^{13}C and ^{15}N lines agree with the X-ray structure. DFT calculations allow the attribution of the NMR peaks to the independent crystallographic sites and the experimental IR bands at low frequencies.

References

[1] Y.Feng, H.Fan, Z.Zhong, H.Wang, D.Qiu . *Inorg. Chem.* , **55** , 11987 (2016).

[2] Y.Feng, M.Li, H.Fan, Q.Huang, D.Qiu, H.Shi . *Dalton Trans.* , **44** , 894 (2015).

[3] C.Duan, H.Zhang, F.Li, J.Xiao, S.Luo, H.Xi . *Soft Matter* , **14** , 9589 (2018).

[4] C.Duan, F.Li, M.Yang, H.Zhang, Y.Wu, H.Xi . *Ind. Eng. Chem. Res.* , **57** , 15385 (2018).

[5] D.M. Chen, N.N. Zhang, C.S. Liu, M.Du . *J. Mater. Chem. C* , **5** , 2311 (2017).

[6] B.Wu, C.A.Davey . *J. Mol. Biol.* , **398**, 633 (2010) 633–640.

[7] L.J.Boerner, J.M.Zaleski . *Curr. Opin. Chem. Biol.* , **9** , 135 (2005).

[8] C.-W.Hsu, S.-M.Chuang, W.-L.Wu, M.-H.Hou . *PLoS ONE* , **7** , e43792 (2012).

[9] L.Rulíšek, J.Šponer . *J. Phys. Chem. B* , **107** , 1913 (2003).

[10] Y.P.Yurenko, J.Novotný, V.Sklenář, R.Marek . *Phys. Chem. Chem. Phys.* , **16** , 2072 (2014).

[11] B.Zambelli, F.Musiani, S.Ciurli . *Metal Ions Life Sci.* , **10** , 135 (2012).

[12] M.H.Shamsi, H.-B.Kraatz . *J. Inorg. Organomet. Polym.* , **23** , 4 (2013).

[13] C.Payus, T.S.Ying, W. N.Kui . *Res. J. Environ. Toxicol.* , **10** , 193 (2016).

[14] (a) J.An, S.J.Geib, N.L.Rosi . *J. Am. Chem. Soc.* , **132** , 38 (2010).

(b) S.Verma, A.Kumar-Mishra, J.Kumar . *Acc. Chem. Res.* , **43** , 79 (2010).

(c) J.Kumar, S.Verma . *Inorg. Chem.* , **48** , 6350 (2009).

(d) F.Zamora, M.P.Amo-Ochoa, P.J.Sanz-Miguel, O.Castillo . *Inorg. Chim. Acta* , **362** , 691 (2009).

(e) J.P.García-Terán, O.Castillo, A.Luque, U.García-Couceiro, P.Román, L.Lezama . *Inorg. Chem.* , **43** ,4549 (2004).

[15] Z.H.Chohan, M.Arif, M.Sarfraz . *Appl. Organomet. Chem.* , **21** , 294 (2007).

[16] Q.Huang, Z.Pan, P.Wang, Z.Chen, X.Zhang, H.Xu . *Bioorg. Med. Chem. Lett.* , **16** , 3030 (2006).

[17] A.Guha, T.Chattopadhyay, N.D.Paul, M.Mukherjee, S.Goswami, T.K.Mondal, E.Zangrando, D.Das . *Inorg. Chem.* , **51** , 8750 (2012).

[18] A.Guha, K.S.Banu, S.Das, T.Chattopadhyay, R.Sanyal, E.Zangrando, D.Das . *Polyhedron* , **52** , 669 (2013).

[19] N.J.Pace, E.Weerapana . *Biomolecules* , **4** , 419 (2014).

[20] Z.Otwinowsky, W.Minor, In: Methods in Enzymology; C.W.Carter, R.M.J.Sweet (Eds.), Academic Press, New York 1997 p. 307.

[21] (a) A.Altomare, C.Burla, M.Camalli, L.Cascarano, C.Giacovazzo, A.Guagliardi, A.G.G.Moliterni, G.Polidori, R.Spagna . *J. Appl. Cryst.* , **32** , 115 (1999,).

(b) A.Altomare, G.Cascarano, C.Giacovazzo, A.Guagliardi . *J. Appl. Cryst.* , **26** , 343 (1993).

[22] G.M.Sheldrick . *Acta Cryst.* , **C71** , 3 (2015).

[23] S.Mackay, C.Edwards, A.Henderson, C.Gilmore, N.Stewart, K.Shankland, A.Donald, University of Glasgow, Scotland 1997.

[24] D.Waasmaier, A.Kirfel . *Acta Cryst.* , **A51** , 416 (1995).

[25] L.Srinivasan, M.R.Taylor . *Chem. Soc. D: Chem. Comm.* 1668 (1970).

[26] P.J.Toscano, P.T.DiMauro . *Inorganica Chmuca Acta* , **217** , 195 (1994).

[27] A.L.Beauchamp . *Inorganica Chimica Acta* , **91** , 33 (1984).

[28] W.Baur . *Acta Cryst.* , **B30** , 1195 (1974).

[29] J.A.Carrabine, M.Sundaralingam, *J. Am. Chem. Soc.* , **92** , 369 (1970).

[30] A.Terzis, D.Mentzafos . *Inorg. Chem.* , **22** , 1140 (1983).

[31] A.Cherouana, N.Benali-Cherif, L.Bendjeddou . *Acta Cryst.* , **E59** , o180 (2003).

[32] B.Guillot, E.Enrique, L.Huder, C.Jelsch . *Acta Cryst.* , **A70** , C279 (2014).

[33] C.Jelsch, S.Soudani, C.Ben Nasr . *IUCrJ* , ***2*** ,327 (2015).

[34] M.A.Spackman, D.Jayatilaka . *CrystEngComm* , **11** ,19 (2009).

[35] C.Jelsch, B.Guillot, A.Lagoutte, C.Lecomte . *J. Appl. Cryst.* , **38** , 38 (2005).

[36] S.Domagała, B.Fournier, D.Liebschner, B.Guillot, C.Jelsch . *Acta Cryst.* , **A68** , 337 (2012).

[37] M.J.Frisch, G.W.Trucks, H.B.Schlegel, G.E.Scuseria, M.A.Robb, J.R.Cheeseman, G.Scalmani, V.Barone, B.Mennucci, G.A.Petersson, H.Nakatsuji, M.Caricato, X.Li, H.P.Hratchian, A.F.Izmaylov, J.Bloino, G.Zheng, J.L.Sonnenberg, M.Hada, M.Ehara, K.Toyota, R.Fukuda, J.Hasegawa, M.Ishida, T.Nakajima, Y.Honda, O.Kitao, H.Nakai, T.Vreven, J.A.Montgomery Jr., J.E.Peralta, F.Ogliaro, M.Bearpark, J.J.Heyd, E.Brothers, K.N.Kudin, V.N.Staroverov, T.Keith, R.Kobayashi, J.Normand,

K.Raghavachari, A.Rendell, J.C.Burant, S.S.Iyengar, J.Tomasi, M.Cossi, N.Rega, J.M.Millam, M.Klene, J.E.Knox, J.B.Cross, V.Bakken, C.Adamo, J.Jaramillo, R.Gomperts, R.E.Stratmann, O.Yazyev, A.J.Austin, R.Cammi, C.Pomelli, J.W.Ochterski, R.L.Martin, K.Morokuma, V.G.Zakrzewski, G.A.Voth, P.Salvador, J.J.Dannenberg, S.Dapprich, A.D.Daniels, O.Farkas, J.B.Foresman, J.V.Ortiz, J.Cioslowski, D.J.Fox, Gaussian 09,Revision B.01, Gaussian, Inc., Wallingford CT 2010.

[38] M.Belhouchet, M.Bahri, J.M.Savariault, T.Mhiri . *Spectrochim. Acta* , **A61** , 387 (2005).

[39] N.L.Calve, F.Romain, M.H.Limage . *J. Mol. Struct.* , **200** , 131 (1989).

[40] S.Shanmuga Sundara Raj, H.-K.Fun, P.-S.Zhao, F.-F.Jian, L.-D.Lu, X.-J.Yang, X.Wang . *Acta Cryst.* , **C56** , 742 (2000).

[41] K.Kaabi, M.Zeller, C.Ben Nasr . *Elixir Chem. Phys.* , **43** , 6877 (2012).

[42] K.Kaabi, M.Zeller, C.Ben Nasr, *Inorg. Chim. Acta* , **388** , 52 , (2012).

[43] K.Kaabi, A.Rayes, C.Ben Nasr, M.Rzaigui, F.Lefebvre . *Mat. Res. Bull.* , **38** , 741 (2003).

[44] A.Oueslati, C.Ben Nasr, A.Durif, F.Lefebvre . *Mat. Res. Bull.* , **40** , 970 (2005).

[45] K.Nakamoto . Infrared and Raman Spectra of Inorganic and Coordination Compounds, Wiley-Interscience, New York 1986.

[46] A.C.Chapman, L.E.Thirlwell . *Spectrochim. Acta* , **20** , 937 (1964).

[47] F.Scheinmann, L.E.Thirtwel . An Introduction to Spectroscopic Methods for Identification of Organic Compounds, Pergamon Press, New York, vol. 1 1970.

Supplementary Information

Synthesis, crystal structure determination, DFT calculation and Hirshfeld surface analysis of a new Zn(II) complex with the guaninium ligand

Kacim Klai[1], Christian Jelsch[2], Christine Lucas[3], Frédéric Lefebvre[3], Werner Kaminsky[4], Cherif Ben Nasr[1], Kamel Kaabi[1]*

[2] Laboratoire de Chimie des Matériaux, Université de Carthage, Faculté des Sciences de Bizerte, 7021 Zarzouna, Tunisie.

[2] CRM[2], CNRS, Institut Jean Barriol, Université de Lorraine, Vandœuvre les Nancy Cedex, France.

[3] Laboratoire de Chimie Organométallique de Surface (LCOMS), Ecole Supérieure de Chimie Physique Electronique, 69626 Villeurbanne Cedex, France.

[4] Department of Chemistry, BOX 351700 University of Washington Seattle, WA 98195, USA.

*Corresponding e-mail: kamel_kaabi@yahoo.fr

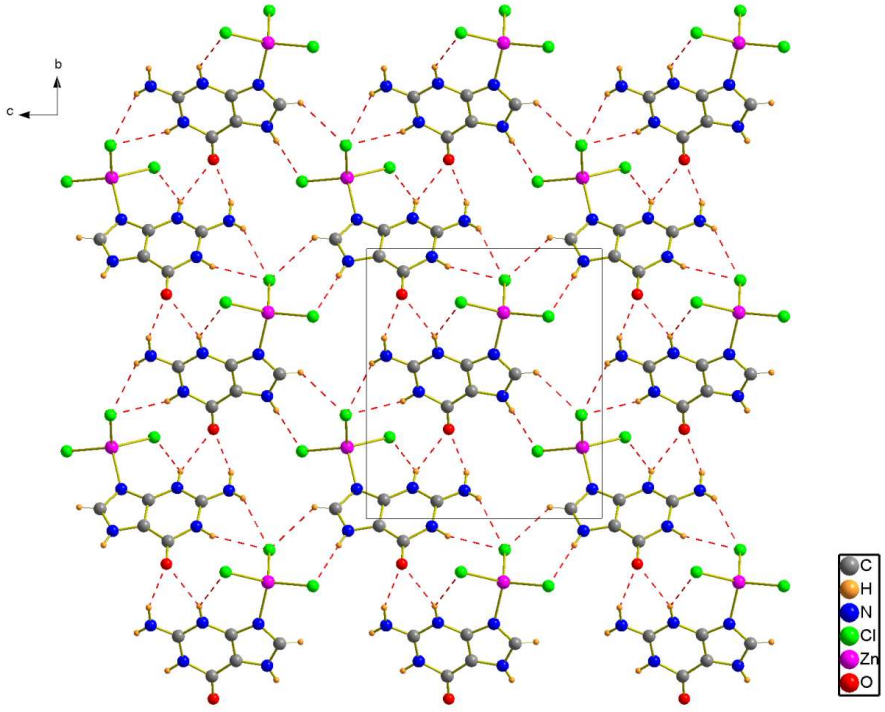

Fig. S1 Projection along the a-axis direction of a layer of $[ZnCl_3(C_5H_6N_5O)]$. Dotted lines indicate hydrogen bonds.

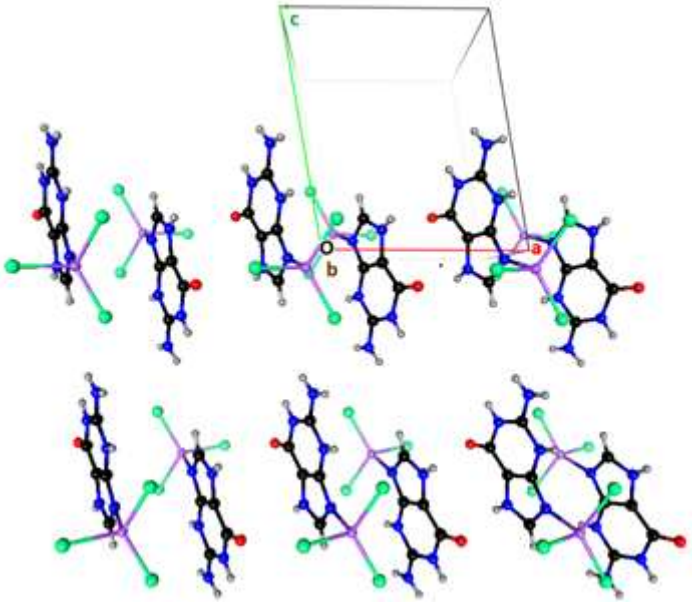

Fig. S2

Autosterogram of the $[ZnCl_3(C_5H_6N_5O)]$ the crystal structure viewed along the *b*-axis

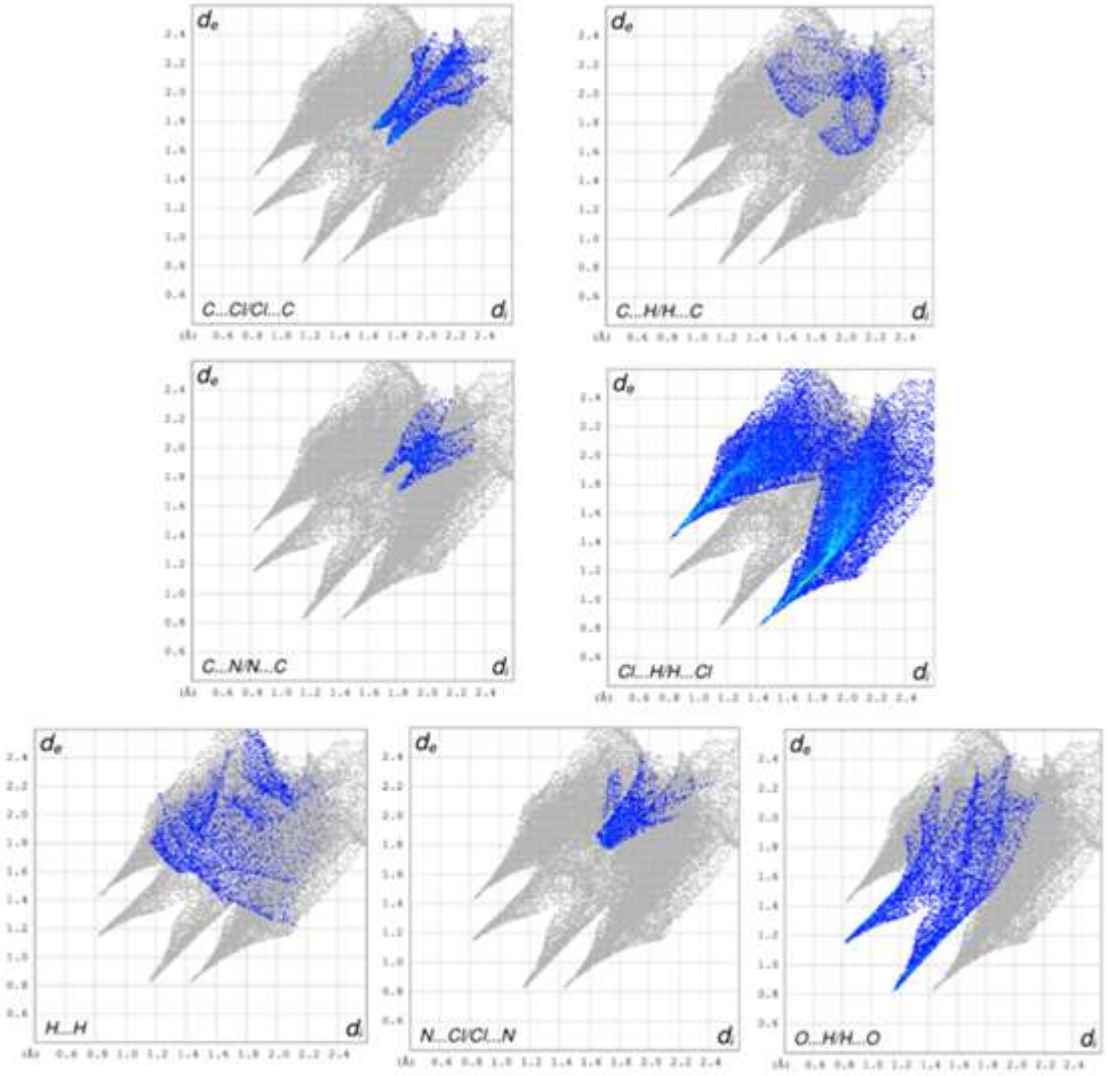

Fig. S3 Fingerprint plots of the Hirshfeld surface around the asymmetric unit (guaninium, $ZnCl_3$).

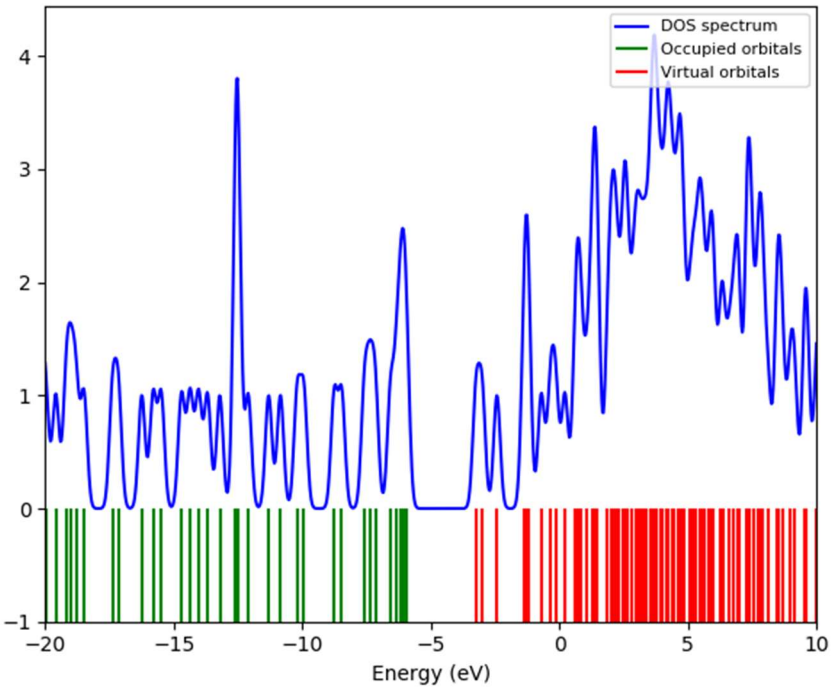

Fig. S4 Energy distribution of the different orbitals for [$ZnCl_2(C_6H_9N_3O_2)$].

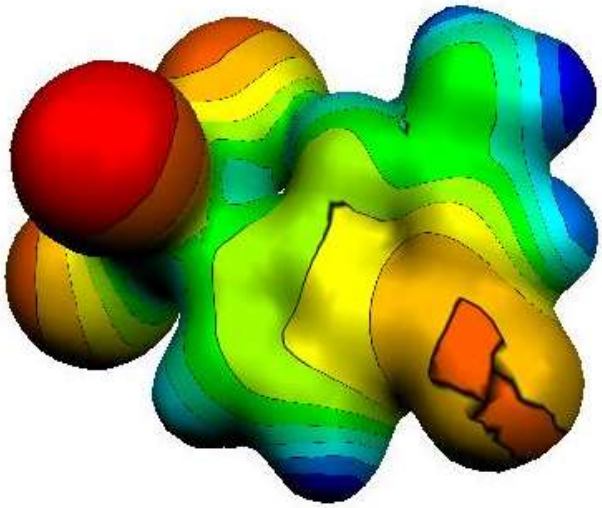

Fig. S5 Molecular Electrostatic Potential of [$ZnCl_3(C_5H_6N_5O)$]

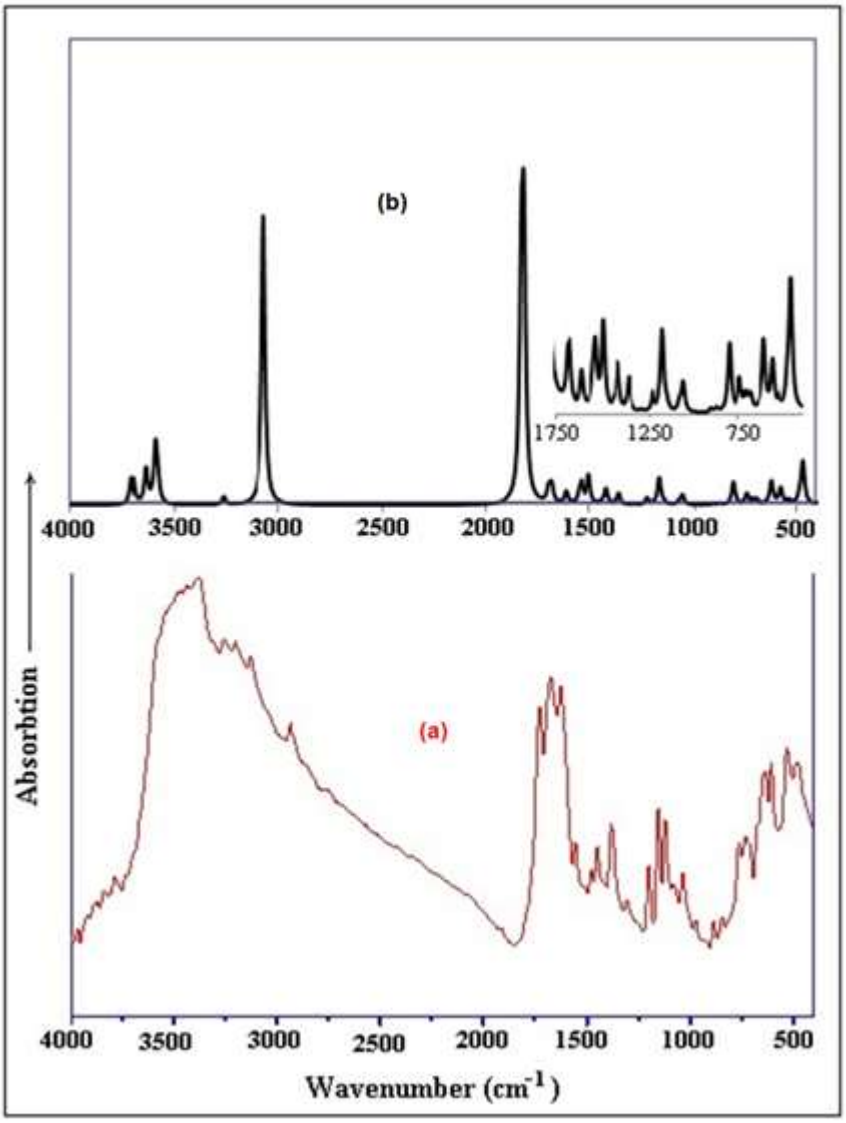

Fig. S6 (a) Experimental and (b) Calculated infrared absorption spectrum of [$ZnCl_3(C_5H_6N_5O)$]

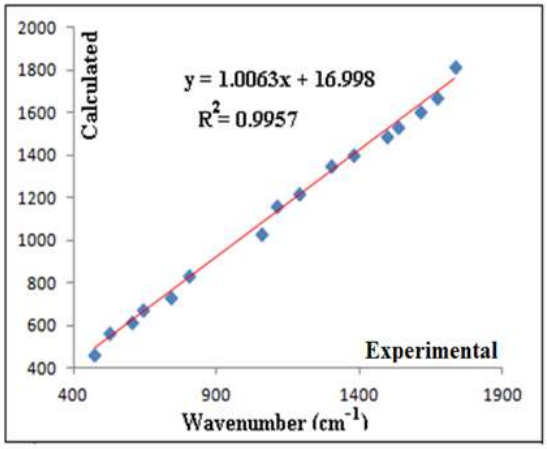

Fig. S7 Comparison between experimental and calculated IR frequencies of [$ZnCl_3(C_5H_6N_5O)$]